8-2017

Ion Channel Signaling Influences Cellular Proliferation and Phagocyte Activity During Axolotl Tail Regeneration

Brandon M. Franklin
University of Kentucky, brandon.franklin57@gmail.com

S. Randal Voss
University of Kentucky, srvoss@uky.edu

Jeffrey L. Osborn
University of Kentucky, jlosbo3@uky.edu

HHS Public Access

Author manuscript

Mech Dev. Author manuscript; available in PMC 2019 February 22.

Published in final edited form as:

Mech Dev. 2017 August ; 146: 42–54. doi:10.1016/j.mod.2017.06.001.

Ion channel signaling influences cellular proliferation and phagocyte activity during axolotl tail regeneration

Brandon M. Franklin, **S. Randal Voss**, and **Jeffrey L. Osborn***

Department of Biology, University of Kentucky, Lexington, KY 40506, United States

Abstract

Little is known about the potential for ion channels to regulate cellular behaviors during tissue regeneration. Here, we utilized an amphibian tail regeneration assay coupled with a chemical genetic screen to identify ion channel antagonists that altered critical cellular processes during regeneration. Inhibition of multiple ion channels either partially (anoctamin1/Tmem16a, anoctamin2/Tmem16b, $K_V2.1$, $K_V2.2$, L-type Ca_V channels and H/K ATPases) or completely (GlyR, $GABA_AR$, $K_V1.5$ and SERCA pumps) inhibited tail regeneration. Partial inhibition of tail regeneration by blocking the calcium activated chloride channels, anoctamin1&2, was associated with a reduction of cellular proliferation in tail muscle and mesenchymal regions. Inhibition of anoctamin 1/2 also altered the post-amputation transcriptional response of p44/42 MAPK signaling pathway genes, including decreased expression of *erk1*/*erk2*. We also found that complete inhibition via voltage gated K^+ channel blockade was associated with diminished phagocyte recruitment to the amputation site. The identification of H^+ pumps as required for axolotl tail regeneration supports findings in *Xenopus* and *Planaria* models, and more generally, the conservation of ion channels as regulators of tissue regeneration. This study provides a preliminary framework for an in-depth investigation of the mechanistic role of ion channels and their potential involvement in regulating cellular proliferation and other processes essential to wound healing, appendage regeneration, and tissue repair.

1. Introduction

Ion channels are known for traditional physiological functions, including muscle contraction, nerve conduction, and maintenance of ionic homeostasis. However, ion channels modulate membrane ion conductance across all cells and tissues, establishing electrical fields (EF) that affect cellular behaviors under normal conditions, during critical periods of development, and in response to tissue injury. Understanding how ion channels function within different biological contexts is central to identifying the molecular basis of channelopathies and for exploiting ion channels for wound healing and tissue repair. Bioelectric signaling via ion channels and control of cellular membrane potentials in planarian and *Xenopus* regeneration have significantly contributed to our understanding of ionic influences on regenerative processes (Levin, 2007; Levin, 2009; Tseng et al., 2010;

*Corresponding author at: Department of Biology, University of Kentucky, 115 Thomas Hunt Morgan, Lexington, KY 40506, United States. jlosbo3@uky.edu (J.L. Osborn).

Supplementary data to this article can be found online at http://dx.doi.org/10.1016/j.mod.2017.06.001.

Levin, 2014). Despite these advances, little is known about the individual channels that are important during regeneration and the specific cellular functions that they influence.

Amphibians and fish provide powerful models to investigate the role of EF and ion channels on cellular processes that are activated during appendage regeneration. Typically in these vertebrates, amputated body parts are flawlessly repaired via the activation, proliferation, and patterning of progenitor cells (McCusker and Gardiner, 2014; Tanaka, 2016). Wound-induced EFs likely affect the behavior of immune and progenitor cells because they are enacted during the early wound-healing response, and interruption or reversal of an EF is detrimental to regeneration (Borgens et al., 1979; Borgens et al., 1977; Jenkins et al., 1996). However, exactly how cells detect and translate EF information to elicit specific cell behaviors is not well understood. One possibility is that information from an EF is modulated and transduced by ion channels. Consistent with this idea, Özkucur et al. (2010)) showed that ion concentrations are modulated in cells near the amputation site during axolotl (*Ambystoma mexicanum*) tail regeneration. This observation suggests that ion channels affect cellular behaviors by regulating ion concentration-dependent signaling cascades during regeneration (Wei et al., 2011; Mao et al., 2009; Wondergem et al., 2001; Wang et al., 2002; Tao et al., 2008).

In this study, we performed a chemical genetic screen to identify ion channels whose functions are required for normal axolotl tail regeneration. We administered tail amputations to axolotl embryos and treated groups with ion channel antagonists. This type of hierarchical drug screen has been previously described, and chemical genetics approaches have proven to be robust for identifying bioelectric mechanisms that affect regeneration (Adams and Levin, 2006; Sengupta et al., 2015). Multiple channels were identified from several ion channel families that either delayed the regenerative process or inhibited the initiation of regeneration. Two of these channels, anoctamin 1 and voltage-gated K^+ channels, were investigated further to determine their effects on cellular proliferation and the activity of phagocytic cells.

2. Methods

2.1. Anesthesia

Experiments were conducted using pre-feeding, hatchling stage axolotl embryos (RRID:AGSC_100H, 9–11 mm in length) obtained from the Ambystoma Genetic Stock Center (RRID:SCR_006372), Department of Biology, University of Kentucky. These nearly mature embryos were removed from chorions immediately before the onset of the experimental protocol. Ethical animal procedures performed in this study were approved by the University of Kentucky IACUC committee (protocol 00907L2005). The skeletal muscle-specific myosin inhibitor N-benzylp-toluene sulfonamide (BTS) was used to anesthetize embryos before all amputations and imaging procedures. This was chosen over benzocaine, a voltage gated Na^+ channel inhibitor, as to not confound the results of the ion channel antagonist being investigated. Embryos were placed in modified Holtfreter's solution (59 mM NaCl, 0.67 mM KCl, 0.76 mM CaCl2, 2.4 mM NaHCO3) with 10 μM BTS at least 15 min before conducting any procedures.

2.2. Regeneration assay

Axolotl tails were imaged under a dissecting microscope and amputated approximately halfway between the tail tip and cloaca (~2 mm). Embryos were then placed in individual wells of a 24-well tissue culture plate with 3 mL of Holtfreter's solution containing various ion channel antagonists or a modified Cl^- free Holtfreter's solution (15 mM $NaC_6H_{11}O_7$, 0.2 mM $KC_6H_{11}O_7$, 0.2 mM $Ca(C_6H_{11}O_7)_2$, 0.2 mM $MgSO_4{\cdot}7H_20$, 0.6 mM $NaHCO_3$). The drug screen consisted of three tiers of ion channel antagonist ranging from broad scale general ion conductance inhibitors (tier 1), to antagonists of ion channel sub families (tier 2), and finally, specific ion channel blockers (tier 3, Table 1). All drugs were initially evaluated at four concentrations (10^{-4}, 10^{-5}, 10^{-6} and 10^{-7} M) with 6 biological replicates for each concentration; some concentrations were lethal and this resulted in $n < 6$ for some drug treatments. Subsequently, ranges of drug concentrations were evaluated on a case-by-case basis and conclusions regarding a drug's impact on regeneration were only drawn from nontoxic concentrations of drugs. Drugs that exhibited systemic toxicity (identified by general atrophy, lethargy and/or tissue degeneration) or lethality at all concentrations were excluded from the study. Lethal or toxic drug concentrations are emphasized in bold in Table 1. At 7 days post-amputation (dpa), embryos were anesthetized, imaged, and tail length was measured. To assess the extent of regeneration, tail length at day 0 (Fig. S1A) was subtracted from tail length at day 7 (Fig. S1B). Following a positive result, drugs were assayed for their impact on normal development in unamputated axolotl embryos and drugs found to adversely affect normal developmental growth were excluded from the study. Results for each pharmacological agent were analyzed in Sigma Plot Statistical Software (SPSS) using a one-way ANOVA with Dunnett's test for post hoc analysis. Significant results were qualitatively assigned as either delayed/reduced regeneration, inhibited regeneration, or toxic/lethal (Fig. S1B–E).

2.3. Phagocyte imaging

Live imaging of phagocytes was accomplished by staining with the non-toxic dye, neutral red. Neutral red stains lysosomes which are present in many cell types but are especially rich in phagocytes such as macrophages. Also, neutral red has been confirmed as an effective and specific stain for macrophages in zebrafish and axolotl using the protocol described below (Herbomel et al., 2001; Davis and Ramakrishnan, 2009; Godwin et al., 2013). Prior to imaging, embryos were placed in Holtfreter's solution containing 5 μg/mL of neutral red dye for 6 h and then de-stained in normal Holtfreter's solution for 24 h. Following this staining/de-staining procedure, embryos were anesthetized and imaged under bright-field (Herbomel et al., 2001; Godwin et al., 2013; Carradice and Lieschke, 2008). Images were quantified by counting all labeled cells within 500 μm of the amputation plane and these values were normalized by tissue section area. Results were analyzed in SPSS using a one-way ANOVA with Dunnett's test for post hoc analysis (control was $t = 0$).

2.4. Proliferation assay

Axolotl embryos were amputated and placed in 24 well plates as outlined above. At 3 dpa, embryos were incubated for 16 h in 10 μM 5-ethynyl-2′-deoxyuridine (EdU), a BrdU analog. After this incubation period, embryos were euthanized and tails were amputated at

the cloaca, immediately fixed in 4% paraformaldehyde, and stored in 70% EtOH. Tissues were then embedded in paraffin wax and cut into 5-micron sagittal sections. The Click-iT® EdU Alexa Fluor® 488 Imaging Kit (C10337, invitrogen) was used to visualize EdU incorporation into the DNA of proliferating cells per the prescribed protocol. Hoechst was used to counter stain the sections. All cells staining positive for EdU incorporation within 500 μm of the amputation plane were counted as well as all cells staining positive for Hoechst within the same anatomical area. Proliferative index was determined by dividing the number of EdU+ cells by the number of Hoechst + cells in each tissue section. Results were analyzed in SPSS using either a one-way ANOVA with Dunnett's test for post hoc analysis or, in the case of tissue specificity analysis, a two-way ANOVA (factors were tissue type and drug treatment) with Student-Newman-Keuls (SNK) test used for post hoc analysis.

2.5. Apoptosis assay

Axolotl embryos were administered tail amputations and placed in 24 well plates and allowed to regenerate for 3 days. Embryos were euthanized and tails were amputated at the cloaca, immediately fixed in 4% paraformaldehyde, and stored in 70% EtOH. Tissues were then embedded in paraffin wax and cut into 5-micron transverse sections. The Click-iT® TUNEL Alexa Fluor® 594 Imaging Kit (C10246, invitrogen) was used to assay for fragmented DNA, a measure of apoptosis (Gavrieli et al., 1992). Tissue sections were grouped as either 0–100 μm or 150–250 μm from the tail tip. TUNEL positive cells in each group were counted and divided by the total number of cells in each group (Hoechst) to give a measure of apoptotic index. Results were analyzed in SPSS using one-way ANOVA and SNK test for post hoc analysis.

2.6. RNA extraction and quantitative real-time PCR

Embryos were administered amputations and placed in 24-well plates as before and allowed to regenerate for 3 days in either modified Holtfreter's or modified Holtfreter's supplemented with the anoctamin 1 inhibitor, T16A(inh)-A01 (10 μM). The distal 1 mm of the tail was re-amputated and collected in ice-cold RNAlater (25 mM $C_6H_7NaO_7$, 10 mM EDTA, 5.3 M $(NH_4)_2SO_4$ and pH 5.2) and stored at −20°C. To isolate mRNA, 2 tails were placed in 100 μL of Trizol, homogenized via sonication, and purified via Zymo Direct-zol™ RNA MiniPrep (R2050) kit and treated with DNase 1. RNA concentration and purity were determined via Nanodrop ND-1000 spectrophotometry (Nanodrop Technologies). cDNA was generated using qScript™ cDNA Supermix (Quanta Biosciences 95,048) and used for PCR. PCR primers were designed using sequence data available on Sal-Site and are listed in Table 2 (Baddar et al., 2015). Quantitative real-time PCR was performed using the StepOnePlus™ Real-Time PCR system (Applied Biosystems®). Samples were loaded into 96-well plates in triplicate with probes and Power SYBR® Green PCR Master Mix (4367659) to detect PCR products. Relative gene expression was calculated using the comparative C_T method ($2^{-\Delta\Delta CT}$) in StepOne software v2.3 per the manufacturer's instructions (Schmittgen and Livak, 2008). Relative quantifications were compared in SPSS using a one-way ANOVA and Student–Newman–Keuls (SNK) method for post hoc analysis.

3. Results

3.1. Pharmacological screen of ion channel groups

3.1.1. Chloride—Nonspecific chloride conductance was examined with the broad-scale Cl^- channel blockers 4,4′-Diisothiocyanatostilbene-2,2′-disulfonic acid (DIDS), 4,4′-dinitrostilbene-2,2′-disulfonic acid (DNDS), and niflumic acid (NFA). Embryos treated with any of these broad scale Cl^- channel antagonists exhibited decreased tail regeneration at all concentrations tested, with the exception of DNDS at 1 μM. For example, embryos exposed to 10 μM DIDS, DNDS, or NFA regenerated 0.71 ± 0.31 mm, 1.11 ± 0.32 mm, and 0.63 ± 0.24 mm respectively, significantly less than untreated embryos (Fig. 1A). Calcium-activated Cl^- channels (CaCC) were evaluated with the family-specific inhibitor CaCCinh-A01. CaCCinh-A01 was lethal at concentrations N2 μM but reduced regeneration at 0.1 μM (1.01 ± 0.24 mm) and 1 μM (1.09 ± 0.17 mm, Fig. 1B) without observable toxic effects. Anoctamins 1&2 (aka Tmem16A/B, Ano1, Ano2) were inhibited with benzbromarone (BBM) or T16a(inh)-A01 (A01). Embryos treated with either BBM or A01 had decreased regenerative capacity at 100 nM (0.56 ± 0.18 mm) and 10 μM (0.88 ± 0.21 mm, Fig. 1C&D). The ligand gated Cl^- channels, $GABA_A$ receptors ($GABA_AR$) and glycine receptors (GlyR), were inhibited with picrotoxin (PTx) and bicuculline methiodide (BCU, $GABA_AR$ only) and both compounds caused reduced regenerative capacity at all concentrations tested. Both PTx (0.645 ± 0.27 mm) and BCU (0.618 ± 0.32 mm) elicited complete inhibition of regeneration at a concentration of 100 μM (Figs. 1E&F). All other Cl^- channel blockers were either toxic or did not affect regeneration (Fig. S2).

3.1.2. Potassium—General potassium conductance was initially examined with the broad-scale K^+ channel blocker tetraethylammonium (TEA). Compared to control embryos (1.83 ± 0.38 mm), TEA treated embryos at a concentration of 1 μM or higher decreased regenerative growth (0.96 ± 0.29 mm, Fig. 2A). The voltage-gated K^+ channel (KV) blocker 4-aminopyridine (4-AP) reduced regenerative outgrowth at 4 μM (1.05 ± 0.03 mm) and completely inhibited regeneration at 10 μM (0.50 ± 0.24 mm) and 100 μM (0.59 ± 0.27 mm, Fig. 2B). $K_V2.1/2.2$ blockade with Guangxitoxin-1E (GTx-1E) slightly reduced regeneration at 1 μM (1.11 ± 0.46, Fig. 4C). $K_V1.5$ blockade with cytochalasin B (CytB) had no effect on regeneration when embryos were incubated at 0.1 or 1 μM, but tail outgrowth was inhibited at 10 μM (0.16 ± 0.11 mm, Fig. 2D). All other K^+ channel blockers used were either toxic or did not affect regeneration (Fig. S3).

3.1.3. Sodium—Sodium was assessed using only tier 2 antagonists as no tier 1 drugs were available (Table 1). The epithelial sodium channel (ENaC) blocker amiloride did not affect regeneration at any concentration tested. The voltage-gated sodium channel (Na_V) antagonists, tetrodotoxin (TTx) and lidocaine, also did not affect regeneration at any concentration tested, although the highest concentration of TTx (100 μM) was lethal in 100% of embryos (Fig. S4).

3.1.4. Calcium—Calcium conductance was examined with the broad-scale Ca^{2+} channel blocker bepridil (BPD). BPD was 100% lethal at every concentration tested. The L, N & T-type calcium channel inhibitor, benidipine HCl (BNP), completely inhibited regeneration at

100 nM (0.60 ± 0.35 mm) and all other concentrations were lethal. L-type channel blockers amlodipine ($Ca_V1.3$) and diltiazem ($Ca_V1.1/1.2/1.4$) diminished the regenerative response, with a maximal effect observed 10 μM (1.03 ± 0.38 mm) and 1 μM (1.04 ± 0.50 mm), respectively. The P & Q-type blocker, ω-conotoxin MVIIC, completely inhibited regeneration with a maximal effect at 10 nM (0.57 ± 0.19 mm). P-type specific inhibitor, ω-agatoxin IVA, had no effect on the regenerative response at any concentration, thus eliminating Q-type channels as affecting regeneration (Fig. S5).

3.2. Pumps/transporters

The sarco/endoplasmic reticulum Ca^{2+}-ATPase (SERCA) was examined with 2,5-di-(tert-butyl)-1,4-benzohydroquinone (tBuBHQ), which completely inhibited regeneration with maximal inhibition at 2 μM (0.41 ± 0.15 mm). Incubation with the H+/K+-ATPase inhibitor, pantoprazole, resulted in a slight reduction of regenerative growth at 100 μM (1.14 ± 0.05 mm). All other transporter inhibitors used were either toxic or did not affect regeneration (Fig. S6).

3.3. Phagocyte activation is dependent on K_V channel signaling

Macrophage activation is required for regeneration to proceed normally and K_V channels are known to influence many functions of macrophages in vitro (Godwin et al., 2013; Kotecha and Schlichter, 1999; Moreno et al., 2013; Qiu et al., 2002; Vicente et al., 2005; Li et al., 2016). This suggests that K_V's may influence tail regeneration through modulation of the macrophage response. To test this hypothesis, it was first necessary to characterize the normal response of phagocytic cells during tail regeneration. Using neutral red (NR) to label phagocytic cells, a significant accumulation of phagocytes was observed at the wound site beginning 24 hours post amputation (hpa, 90.1 ± 20.8 NR+ cells/mm^2 tissue) and initially peaking at 48 hpa (189.2 ± 53.7 NR+ cells/mm^2 tissue). This was followed by a decline concurrent with tissue outgrowth and then a second peak at 144 hpa (200.6 ± 34.4 NR+ cells/mm^2 tissue, Fig. 3). NR stained cells were confirmed to be phagocytic by repeating the NR staining procedure on embryos that had been previously injected with liposome encapsulated clodronate. In comparison to control embryos, clodronate treated embryos exhibited a significant reduction of NR+ cells (Fig. S7).

While CytB is a potent inhibitor of $K_V1.5$ channel activity, it has off target effects, such as disruption of actin polymerization that could also influence regeneration. To further assess the role of K_V channels on phagocyte activity we used an alternate K_V channel blocker, 4-AP. Embryos were incubated at 2 concentrations of 4-AP (5 μM and 25 μM) beginning at 12 hpa and harvested at either 3 or 6 days post amputation (dpa). At 3 dpa, embryos incubated in either 5 μM (45.88 ± 12.35 NR+ cells) or 25 μM (46.63 ± 10.07 NR+ cells) exhibited a marked reduction in phagocyte recruitment to the wound site compared to control embryos (123.33 ± 15.67 NR+ cells) but there was no difference between the two concentrations tested. At 6 dpa, the reduction of phagocyte recruitment persisted compared to control (190.29 ± 43.02 NR+ cells) and there was a concentration dependent response between the 5 μM group (102.38 ± 9.89 NR+ cells) and 25 μM group (52.71 ± 14.74 NR+ cells, Fig. 4). To confirm this result, embryos were subjected to one of three treatments: (1) Encapsome®/Fluorosome®-DiI 50:50 mixture IP injection 24 h before amputation (24hba), (2)

Clodrosome®/Fluorosome®-DiI 50:50 mixture IP injection 24hba or (3) Encapsome®/Fluorosome®-DiI 50:50 mixture IP injection 24hba and incubation in 25 μM 4-AP beginning at 12 hpa. Embryos were then harvested at 3 dpa and whole mount imaged under fluorescent and bright field conditions. Embryos subjected to both the phagocyte depletion protocol (17.045 ± 17.30 DiI+ cells/mm^2) and K_V channel inhibition (31.80 ± 19.35 DiI+ cells/mm^2) exhibited reduced phagocyte recruitment following amputation compared to control conditions (145.20 ± 77.17 DiI+ cells/mm^2, Fig. 5). Notably, the number of phagocytes at the amputation site at 3 dpa under control conditions identified by Fluorosome®-DiI incorporation was consistent with the number identified by NR staining at the same time point.

3.4. Anoctamin 1 blockade delays regeneration via inhibition of proliferation

Cell proliferative responses to amputation were assessed by measuring EdU incorporation at 3 dpa under several experimental interventions. EdU incorporation was observed in 34.00 ± 6.44% of cells within 500 μm of the amputation plane under control conditions (n = 4, Fig. 6 A–A″ & C). In contrast, broad-scale Cl^- channel blockade (DIDS: n = 4, 18.13 ± 5.52%& DNDS: n = 5, 19.65 ± 9.29%, Fig. 6C) or specific inhibition of anoctamin 1 (A01: n = 5, 19.65 ± 4.54%, Fig. 6 B–B″ & C) significantly reduced the percentage of cells proliferating within this same anatomical area. Embryos incubated in Cl^- free Holtfreter's exhibited a trend towards reduced proliferation (24.80 ± 9.74%, n = 5, Fig. 6C) but the difference was not statistically significant relative to controls. We note that apoptosis was assessed using a TUNEL assay; no differences were observed between embryos subjected to anoctamin 1 blockade and controls (Fig. 7).

To more finely examine proliferation spatially, cell counts were obtained for epidermal (ED), spinal cord (SC), and mesenchymal & muscle (MM) regions of the tail. Neither broad-scale Cl^- channel blockade (DIDS & DNDS) nor anoctamin 1 inhibition (A01) treatments affected proliferation rates within the ED and SC tissues; the reduced proliferation response was only observed in MM tissues. These results suggest that functional chloride flux mediated by Ano1 is critical for regulating the proliferative response in the mesenchyme but not in other tissues (Fig. 6 D&E).

3.5. Anoctamin 1 blockade diminishes activation of p44/42 MAPK signaling pathway

To investigate gene expression changes associated with anoctamin 1 inhibition of tail regeneration, quantitative real-time PCR was used to measure mRNA expression of p44/42 MAPK signaling pathway genes, a pathway activated during cellular proliferation. After amputation, *pkcγ*, *mek1*, *mek2*, *erk1* and *erk2* showed a higher percent increase in transcription in control embryos vs anoctamin 1 treated embryos at 3 dpa. In contrast, expression was downregulated more strongly in control embryos than embryos subjected to anoctamin 1 inhibition by A01 at 3 dpa for early p44/42 pathway genes (*pkcα*, *pkcβ*, *rras* and *raf1*) (Fig. 8). These results show that anoctamin 1 affects the transcription of p44/42 MAPK pathway genes that regulate cellular proliferation.

4. Discussion

In this study, we identified ion channel antagonists that partially (anoctamin1/Tmem16a, anoctamin2/Tmem16b, $K_V2.1$, $K_V2.2$, L-type Ca_V channels and H/K ATPases) or completely (GlyR, $GABA_AR$, $K_V1.5$ and SERCA pumps) inhibited axolotl tail regeneration. Below we separately discuss the affected ion channels from each of these categories (Fig. 9).

4.1. Partially inhibiting channels & transporters

4.1.1. Anoctamins 1/2 (Tmem16A/B)—Our results suggest a role for CaCCs in the tail regeneration process. Regeneration was delayed when embryos were subjected to either broad-scale Cl^- channel blockade (DIDS, DNDS & niflumic acid) or CaCC inhibition (CaCCinh-A01, T16a(inh)-A01 & Benzbromarone). CaCC currents were described over 25 years ago but their molecular basis was only recently discovered (Hartzell et al., 2005). In 2008, three independent researchers identified anoctamin 1 and anoctamin 2 channels as mediators of CaCC currents (Caputo et al., 2008; Schroeder et al., 2008; Yang et al., 2008). Anoctamin 1 was first discovered as an overexpression marker for gastrointestinal stromal tumors (then known as DOG1) and has since been shown to promote other forms of cancer (Britschgi et al., 2013; West et al., 2004). Blockade of anoctamin 1 suppresses tumor growth and invasion in multiple human cancer lines (Jia et al., 2015; Liu et al., 2012). There is evidence that anoctamin 1 manifested these effects through regulation of both cell migration and proliferation (Qu et al., 2014; Ruiz et al., 2012). Our results support this idea because inhibition of anoctamin 1 significantly decreased the number of proliferating cells in the regenerating tail. This suggests that anoctamin 1 channel function is directly or indirectly required to sustain cell proliferation at a level that is typical of normal tail regeneration.

Our results further suggest that anoctamin 1 affected tail regeneration by modulating the p44/42 MAPK pathway, which is a well-known regulator of cell proliferation (Zhang and Liu, 2002). Following tail amputation, Erk1/2 signaling pathway genes were transcriptionally upregulated to a higher degree in control embryos than embryos treated with anoctamin 1 antagonist. Thus, the magnitude of *erk1*/*erk2* transcription correlated on one hand with anoctamin 1 function, and conversely, with the magnitude of cell proliferation. We propose the following model: anoctamin 1, activated by an initial calcium surge, acts as a countercurrent ion channel to amplify calcium signaling. This amplified surge subsequently activates the Erk1/2 pathway leading to increased cellular proliferation. This model assumes there is a burst in intracellular $[Ca^{2+}]$ following tail amputation and a dependence of intracellular Ca^{2+} flux on chloride conductance. Özkucur et al. (2010) downplayed the role of Ca^{2+} in their model of axolotl tail regeneration. However, they reported significant increases in Ca^{2+} fluorescence at 48 hpa, preceding the time when the tail shows measureable regenerative outgrowth. This Ca^{2+} flux at 48 hpa supports our proposed model (Özkucur et al., 2010; Barro-Soria et al., 2010; Wang and van Breemen, 1999).

4.1.2. $K_V2.1/2.2$—K_V2 channel blockade with TEA or GTx-1E also reduced regeneration. K_V2 channels traditionally act as the primary delayed rectifier involved in regulating the excitability of neurons and facilitating exocytosis in neurons and

neuroendocrine cells (Feinshreiber et al., 2009; Misonou et al., 2005). These functions of K_V2 channels could be associated with the release of neurotrophic factors that are required for regeneration, the so-called neurotrophic requirement for regeneration (Kumar and Brockes, 2012; Singer, 1974). However, it is also important to consider the direct influence of K_V2 channels on the cellular dynamics of non-excitable cells (Kumar and Brockes, 2012). K_V2 acts as a promoter of cell migration in cultured HEK293, CHO, and bone derived mesenchymal stem cells (MSC) via phosphorylation of focal adhesion kinase (Hu et al., 2011; Wei et al., 2008). MSCs also require functioning K_V2 channels for proper progression through the cell cycle by facilitating plasma membrane-endoplasmic reticulum contact sites (Cobb et al., 2015; Deng et al., 2007). These MSC specific characteristics of K_V2 channels are particularly interesting considering their resemblance to progenitor cells of the blastema, but more research is required to determine the specific role of K_V2 channels within the context of appendage regeneration.

4.2. L-type Ca^{2+} channels ($Ca_V1.1–1.4$)

The L-type channel blockers, amlodipine and diltiazem, partially inhibited tail regeneration. These channels are mostly known for their roles in excitable cells, where they couple plasma membrane depolarization with increases in Ca^{2+} conductance across the membrane. Recent evidence also suggests that they are important physiological components of many non-excitable cell types (Davenport et al., 2015; Wen et al., 2012). Ca^{2+} is a ubiquitous second messenger in all cell types and can influence many different cellular processes (Berridge, 1995; Berridge et al., 2000; Clapham, 2007; Zayzafoon, 2006; Zheng and Poo, 2007). Because of the widespread nature of L-type Ca^{2+} channel expression and the complicated features of intracellular Ca^{2+} signaling, these channels may not present the best targets for future investigations. But, if the model we proposed above is correct, the anoctamin 1/2 Cl^- channels may provide an indirect path to modulate intracellular calcium flux in a specific cell population.

4.2.1. H^+/K^+ ATPases—Our study found that H^+ pump inhibition with pantoprazole sodium reduced regenerative outgrowth. Proton pumps have been classically associated with their roles in gastric and renal function. However, over the past several decades they have been identified as critical mediators of wound healing and regeneration (Adams et al., 2007; Walan et al., 1989; Balestrini et al., 2017). Most of this influence has been attributed to the proton pump's involvement in establishing and maintaining trans-epithelial electrical potentials that drive wound-induced electrical fields (Nuccitelli, 2003). A recent chemical genetic screen performed using planarian head regeneration also identified H^+/K^+ ATPase as important for initiating the regenerative process through control of cellular membrane potentials (V_{mem}) (Beane et al., 2011). H^+ pump driven changes in V_{mem} are required for regeneration to proceed normally in the *Xenopus* model of regeneration (Adams et al., 2007). Our findings further validate the requirement of H^+ pumps in organisms capable of appendage regeneration.

4.3. Inhibiting channels & transporters

4.3.1. $K_V1.5$—Blockade of $K_V1.5$ with 4-AP or CytB resulted in a robust and concentration dependent total inhibition of regeneration. These channels are widely

expressed in a large number of tissues and are involved in regulating V_{mem} and electrophysiological properties of a variety of cell types (Archer et al., 1998; Olson et al., 2006; Tabarean, 2014). In addition to these electrophysiological functions, $K_V1.5$ channels have been implicated in regulating cell cycle progression and migration (Kotecha and Schlichter, 1999; Vallejo-Gracia et al., 2013; Villalonga et al., 2008). Of particular interest is their role in regulating immune cell dynamics. Macrophages are required for amphibian regeneration and the invertebrate homologue of macrophages (hemocytes) respond to exogenously applied electrical fields in vivo in a K_V dependent manner (Godwin et al., 2013; Franklin et al., 2016). Consistent with this line of reasoning, phagocyte activation was severely diminished during tail regeneration after K_V channel blockade with 4-AP. This suggests that K_V channels may be critical regulators of macrophage/monocyte populations during regeneration. However, further studies are necessary to further clarify the role for K_v channels in macrophage activation during tissue regeneration and whether or not this mechanism is a cell autonomous.

4.3.2. GlyR/GABA$_A$R—GlyR and GABA$_A$R blockade with picrotoxin or bicuculline resulted in strong inhibition of regeneration at relatively low concentrations. These ligand-gated chloride channels act primarily as receptors for inhibitory neurotransmitters in the CNS, with GABA$_A$R acting mostly in the brain and GlyR functioning primarily in the brainstem and spinal cord (Lynch, 2004; Sigel and Steinmann, 2012). This immediately implicates nerves and their required neurotrophic factors for appendage regeneration since modulation of either of these receptors would disrupt normal neuronal activity during regeneration. There is evidence that these receptors influence neural progenitor cells during early development and regulate many critical cellular processes in multiple cell types, mostly via modulation of intracellular Ca^{2+} concentrations (Nguyen et al., 2001; Van Den Eynden et al., 2009). Importantly, misexpression of GlyR has recently been shown to disrupt patterning and development in neural, muscle and vascular tissues via physiological modulation of membrane potentials (Lobikin et al., 2012; Lobikin et al., 2014; Pai et al., 2015). It will be interesting to examine the expression patterns of these receptors in cells of regenerating axolotl tissues to see if they are altered following tissue injury. More research will be necessary to assess the exact role of GlyR/GABA$_A$R during axolotl regeneration.

4.3.3. SERCA pump—SERCA inhibition with tBuBHQ completely inhibited regeneration at low concentrations, although higher concentrations of this drug were lethal. The sacroplasmic/endoplasmic reticulum Ca^{2+} ATPase (SERCA) is expressed in virtually all cell types and distributes Ca^{2+} ions against their concentration gradient into sarcoplasmic and endoplasmic reticula. This allows for quick sequestration of cytoplasmic free Ca^{2+} following a Ca^{2+} signaling event and for the generation of intracellular calcium stores that allow for a more rapid and robust Ca^{2+} surge upon cellular stimulation (Wuytack et al., 2002). As discussed above, Ca^{2+} signaling is associated with many cytosolic signaling pathways and physiological functions, all of which require precise control of intracellular Ca^{2+} concentration pulses in terms of both magnitude and duration, and these Ca^{2+} dependent pathways are operative in models of epimorphic regeneration (Berridge et al., 2000; Rao et al., 2014). The ubiquitous nature of SERCA expression may explain why inhibition of this ion channel completely inhibited regeneration, while incomplete

regeneration was observed for L-type Ca_V channel inhibition. Based on the extensive network of pathways influenced by Ca^{2+} signaling and the pervasive nature of SERCA pumps, SERCA pumps will present challenging targets to investigate mechanisms of tissue regeneration.

5. Summary

A chemical genetic screen was performed to identify ion channel antagonists that inhibit axolotl tail regeneration. Then, experiments were performed to determine how select antagonists affected cellular behaviors (cell proliferation and phagocyte activation) that are required for successful tail regeneration. The antagonists that were identified from the screen targeted the following ion channels: anoctamins 1/2 (Tmem16a/b), GlyR, $GABA_AR$, $K_V1.5$, $K_V2.1$, $K_V2.2$, L-type Ca_V channels, H/K ATPases and SERCA pumps. An association was established between K_V channel blockade and phagocyte activation, and thus a possible mechanism for K_V channel mediated inhibition of axolotl tail regeneration. Also, blockade of the anoctamins reduced cellular proliferation, and this was associated with modulated transcription of Erk1/2 signaling pathway genes. It has been shown previously that the transcriptional response to bioelectric signaling is conserved among axolotl regeneration, Xenopus development and human progenitor cells (Pai et al., 2015). This speaks to the broad relevance of the data presented in this report and lends credence to the idea that the antagonists and ion channels prioritized from our study will provide useful tools and targets for investigating mechanisms of tissue regeneration.

Supplementary Material

Refer to Web version on PubMed Central for supplementary material.

Acknowledgements

This work was funded by the Biomedical Sciences Research Group, LLC and the NIH (R24OD021479). Axolotl embryos used in this study were obtained from the Ambystoma Genetic Stock Center (AGSC) at the University of Kentucky. The AGSC is funded by the NIH (P40OD019794). The Authors would like to thank Deirdre Mcdonnell, for her expertise in quantitative PCR and other general lab work that contributed to this project.

References

Adams DS, Levin M, 2006 Inverse drug screens: a rapid and inexpensive method for implicating molecular targets. Genesis 44 (11), 530–540. [PubMed: 17078061]

Adams DS, Masi A, Levin M, 2007 H+ pump-dependent changes in membrane voltage are an early mechanism necessary and sufficient to induce Xenopus tail regeneration. Development 134 (7), 1323–1335. [PubMed: 17329365]

Archer SL, et al., 1998 Molecular identification of the role of voltage-gated K+ channels, Kv1. 5 and Kv2. 1, in hypoxic pulmonary vasoconstriction and control of resting membrane potential in rat pulmonary artery myocytes. J. Clin. Inv 101 (11), 2319.

Baddar NWAH, et al., 2015 Sal-site: research resources for the Mexican Axolotl In: Kumar A, Simon A (Eds.), Salamanders in Regeneration Research: Methods and Protocols. Springer New York, New York, NY, pp. 321–336.

Balestrini L, et al., 2017 The natural compound sanguinarine perturbs the regenerative capabilities of planarians. Int. J. Dev. Biol 61 (1–2), 43–52. [PubMed: 28287246]

Barro-Soria R, et al., 2010 ER-localized bestrophin 1 activates Ca2+-dependent ion channels TMEM16A and SK4 possibly by acting as a counterion channel. Pflugers Arch. 459 (3), 485–497. [PubMed: 19823864]

Beane WS, et al., 2011 A chemical genetics approach reveals H,K-ATPase-mediated membrane voltage is required for planarian head regeneration. Chem. Biol 18 (1), 77–89. [PubMed: 21276941]

Berridge MJ, 1995 Calcium signalling and cell proliferation. BioEssays 17 (6), 491–500. [PubMed: 7575490]

Berridge MJ, Lipp P, Bootman MD, 2000 The versatility and universality of calcium signalling. Nat. Rev. Mol. Cell. Biol 1 (1), 11–21. [PubMed: 11413485]

Borgens RB, Vanable JW, Jaffe LF, 1977 Bioelectricity and regeneration: large currents leave the stumps of regenerating newt limbs. Proc. Natl. Acad. Sci 74 (10), 4528–4532. [PubMed: 270701]

Borgens RB, Vanable JW, Jr., Jaffe LF, 1979 Role of subdermal current shunts in the failure of frogs to regenerate. J. Exp. Zool 209 (1), 49–56. [PubMed: 314968]

Britschgi A, et al., 2013 Calcium-activated chloride channel ANO1 promotes breast cancer progression by activating EGFR and CAMK signaling. Proc. Natl. Acad. Sci. U. S. A 110 (11), E1026–E1034. [PubMed: 23431153]

Caputo A, et al., 2008 TMEM16A, a membrane protein associated with calcium-dependent chloride channel activity. Science 322 (5901), 590–594. [PubMed: 18772398]

Carradice D, Lieschke GJ, 2008 Zebrafish in hematology: sushi or science? Blood 111 (7), 3331–3342. [PubMed: 18182572]

Clapham DE, 2007 Calcium Signaling. Cell 131 (6), 1047–1058. [PubMed: 18083096]

Cobb MM, et al., 2015 Cell cycle-dependent changes in localization and phosphorylation of the plasma membrane Kv2.1 K+ channel impact endoplasmic reticulum membrane contact sites in COS-1 cells. J. Biol. Chem 290 (49), 29189–29201. [PubMed: 26442584]

Davenport B, et al., 2015 Signature channels of excitability no more: L-type channels in immune cells. Front. Immunol 6, 375. [PubMed: 26257741]

Davis JM, Ramakrishnan L, 2009 The role of the granuloma in expansion and dissemination of early tuberculous infection. Cell 136 (1), 37–49. [PubMed: 19135887]

Deng XL, et al., 2007 Cell cycle-dependent expression of potassium channels and cell proliferation in rat mesenchymal stem cells from bone marrow. Cell Prolif. 40 (5), 656–670. [PubMed: 17877608]

Feinshreiber L, et al., 2009 Voltage-gated potassium channel as a facilitator of exocytosis. Ann. N. Y. Acad. Sci 1152, 87–92. [PubMed: 19161379]

Franklin BM, Maroudas E, Osborn JL, 2016 Sine-wave electrical stimulation initiates a voltage-gated potassium channel-dependent soft tissue response characterized by induction of hemocyte recruitment and collagen deposition. Physiol. Rep 4 (12).

Gavrieli Y, Sherman Y, Ben-Sasson SA, 1992 Identification of programmed cell death in situ via specific labeling of nuclear DNA fragmentation. J. Cell Biol 119 (3), 493–501. [PubMed: 1400587]

Godwin JW, Pinto AR, Rosenthal NA, 2013 Macrophages are required for adult salamander limb regeneration. Proc. Natl. Acad. Sci 110 (23), 9415–9420. [PubMed: 23690624]

Hartzell C, Putzier I, Arreola J, 2005 Calcium-activated chloride channels. Annu. Rev. Physiol 67 (1), 719–758. [PubMed: 15709976]

Herbomel P, Thisse B, Thisse C, 2001 Zebrafish early macrophages colonize cephalic mesenchyme and developing brain, retina, and epidermis through a M-CSF receptor-dependent invasive process. Dev. Biol 238 (2), 274–288. [PubMed: 11784010]

Hu X, et al., 2011 Hypoxic preconditioning enhances bone marrow mesenchymal stem cell migration via Kv2.1 channel and FAK activation. Am. J. Physiol. Cell Physiol 301 (2), C362–C372. [PubMed: 21562308]

Jenkins LS, Duerstock BS, Borgens RB, 1996 Reduction of the current of injury leaving the amputation inhibits limb regeneration in the red spotted newt. Dev. Biol 178 (2), 251–262. [PubMed: 8812127]

Jia L, et al., 2015 Inhibition of calcium-activated chloride channel ANO1/TMEM16A suppresses tumor growth and invasion in human lung cancer. PLoS One 10 (8), e0136584. [PubMed: 26305547]

Kotecha SA, Schlichter LC, 1999 A Kv1.5 to Kv1.3 switch in endogenous hippocampal microglia and a role in proliferation. J. Neurosci 19 (24), 10680–10693. [PubMed: 10594052]

Kumar A, Brockes JP, 2012 Nerve dependence in tissue, organ, and appendage regeneration. Trends Neurosci. 35 (11), 691–699. [PubMed: 22989534]

Levin M, 2007 Large-scale biophysics: ion flows and regeneration. Trends Cell Biol. 17 (6), 261–270. [PubMed: 17498955]

Levin M, 2009 Bioelectric mechanisms in regeneration: unique aspects and future perspectives Seminars in Cell & Developmental Biology. Elsevier.

Levin M, 2014 Endogenous bioelectrical networks store non-genetic patterning information during development and regeneration. J. Physiol 592 (11), 2295–2305. [PubMed: 24882814]

Li C, Levin M, Kaplan DL, 2016 Bioelectric modulation of macrophage polarization. Sci Rep 6, 21044. [PubMed: 26869018]

Liu W, et al., 2012 Inhibition of Ca2+-activated Cl− channel ANO1/TMEM16A expression suppresses tumor growth and invasiveness in human prostate carcinoma. Cancer Lett. 326 (1), 41–51. [PubMed: 22820160]

Lobikin M, et al., 2012 Resting potential, oncogene-induced tumorigenesis, and metastasis: the bioelectric basis of cancer in vivo. Phys. Biol 9 (6), 065002.

Lobikin M, et al., 2014 Selective depolarization of transmembrane potential alters muscle patterning and muscle cell localization in Xenopus laevis embryos. Int. J. Dev. Biol 59 (7–9), 303–311.

Lynch JW, 2004 Molecular structure and function of the glycine receptor chloride channel. Physiol. Rev 84 (4), 1051–1095. [PubMed: 15383648]

Mao J, et al., 2009 Volume-activated chloride channels contribute to cell-cycle-dependent regulation of HeLa cell migration. Biochem. Pharmacol 77 (2), 159–168. [PubMed: 18992227]

McCusker CD, Gardiner DM, 2014 Understanding positional cues in salamander limb regeneration: implications for optimizing cell-based regenerative therapies. Dis. Model. Mech 7 (6), 593–599. [PubMed: 24872456]

Misonou H, Mohapatra DP, Trimmer JS, 2005 Kv2.1: a voltage-gated k+ channel critical to dynamic control of neuronal excitability. Neurotoxicology 26 (5), 743–752. [PubMed: 15950285]

Moreno C, et al., 2013 Modulation of voltage-dependent and inward rectifier potassium channels by 15-epi-lipoxin-A4 in activated murine macrophages: implications in innate immunity. J. Immunol 191 (12), 6136–6146. [PubMed: 24249731]

Nguyen L, et al., 2001 Neurotransmitters as early signals for central nervous system development. Cell Tissue Res. 305 (2), 187–202. [PubMed: 11545256]

Nuccitelli R, 2003 Endogenous electric fields in embryos during development, regeneration and wound healing. Radiat. Prot. Dosim 106 (4), 375–383.

Olson TM, et al., 2006 Kv1. 5 channelopathy due to KCNA5 loss-of-function mutation causes human atrial fibrillation. Hum. Mol. Genet 15 (14), 2185–2191. [PubMed: 16772329]

Özkucur N, Epperlein H-H, Funk RHW, 2010 Ion imaging during axolotl tail regeneration in vivo. Dev. Dyn 239 (7), 2048–2057. [PubMed: 20549718]

Pai VP, et al., 2015 Endogenous gradients of resting potential instructively pattern embryonic neural tissue via notch signaling and regulation of proliferation. J. Neurosci 35 (10), 4366–4385. [PubMed: 25762681]

Qiu MR, Campbell TJ, Breit SN, 2002 A potassium ion channel is involved in cytokine production by activated human macrophages. Clin. Exp. Immunol 130 (1), 67–74. [PubMed: 12296855]

Qu Z, et al., 2014 The Ca2+-activated Cl− channel, ANO1 (TMEM16A), is a double-edged sword in cell proliferation and tumorigenesis. Cancer Med. 3 (3), 453–461. [PubMed: 24639373]

Rao N, et al., 2014 Proteomic analysis of fibroblastema formation in regenerating hind limbs of Xenopus laevis froglets and comparison to axolotl. BMC Dev. Biol 14 (1), 32. [PubMed: 25063185]

Ruiz C, et al., 2012 Enhanced expression of ANO1 in head and neck squamous cell carcinoma causes cell migration and correlates with poor prognosis. PLoS One 7 (8), e43265. [PubMed: 22912841]

Schmittgen TD, Livak KJ, 2008 Analyzing real-time PCR data by the comparative CT method. Nat. Protocol 3 (6), 1101–1108.

Schroeder BC, et al., 2008 Expression cloning of TMEM16A as a calcium-activated chlo-ride channel subunit. Cell 134 (6), 1019–1029. [PubMed: 18805094]

Sengupta S, Zhang L, Mumm JS, 2015 Chemical genetics and regeneration. Future Med. Chem 7 (16), 2263–2283. [PubMed: 26511866]

Sigel E, Steinmann ME, 2012 Structure, function, and modulation of GABAA receptors. J. Biol. Chem 287 (48), 40224–40231. [PubMed: 23038269]

Singer M, 1974 Neurotrophic control of limb regeneration in the NEWT*. Ann. N. Y. Acad. Sci 228 (1), 308–321. [PubMed: 4526284]

Tabarean IV, 2014 Electrical remodeling of preoptic GABAergic neurons involves the Kv1.5 subunit. PLoS One 9 (5), e96643. [PubMed: 24797243]

Tanaka Elly M., 2016 The molecular and cellular choreography of appendage regeneration. Cell 165 (7), 1598–1608. [PubMed: 27315477]

Tao R, et al., 2008 Regulation of Cell Proliferation by Intermediate-Conductance Ca2+-Activated Potassium and Volume-Sensitive Chloride Channels in Mouse Mesenchymal Stem Cells. 295 pp. C1409–C1416.

Tseng A-S, et al., 2010 Induction of vertebrate regeneration by a transient sodium current. J. Neurosci 30 (39), 13192–13200. [PubMed: 20881138]

Vallejo-Gracia A, et al., 2013 Emerging role for the voltage-dependent K+ channel Kv1.5 in B-lymphocyte physiology: expression associated with human lymphoma malignancy. J. Leukoc. Biol 94 (4), 779–789. [PubMed: 23847097]

Van Den Eynden J, et al., 2009 Glycine and glycine receptor signalling in non-neuronal cells. Front. Mol. Neurosci 2.

Vicente R, et al., 2005 Pattern of Kv beta subunit expression in macrophages depends upon proliferation and the mode of activation. J. Immunol 174 (8), 4736–4744. [PubMed: 15814698]

Villalonga N, et al., 2008 Cell cycle-dependent expression of Kv1. 5 is involved in myoblast proliferation. Biochim. Biophys. Acta 1783 (5), 728–736. [PubMed: 18230363]

Walan A, et al., 1989 Effect of omeprazole and ranitidine on ulcer healing and relapse rates in patients with benign gastric ulcer. N. Engl. J. Med 320 (2), 69–75. [PubMed: 2643037]

Wang X, van Breemen C, 1999 Depolarization-mediated inhibition of Ca(2+) entry in endothelial cells. Am. J. Phys 277 (4 Pt 2), H1498–H1504.

Wang G-L, et al., 2002 Deficiency in ClC-3 chloride channels prevents rat aortic smooth muscle cell proliferation. Circ. Res 91 (10), e28–e32. [PubMed: 12433844]

Wei J-F, et al., 2008 Formation of Kv2.1-FAK complex as a mechanism of FAK activation, cell polarization and enhanced motility. J. Cell. Physiol 217 (2), 544–557. [PubMed: 18615577]

Wei W-C, et al., 2011 The potassium–chloride cotransporter 2 promotes cervical cancer cell migration and invasion by an ion transport-independent mechanism. J. Physiol 589 (22), 5349–5359. [PubMed: 21911617]

Wen L, et al., 2012 L-type calcium channels play a crucial role in the proliferation and osteogenic differentiation of bone marrow mesenchymal stem cells. Biochem. Biophys. Res. Commun 424 (3), 439–445. [PubMed: 22771798]

West RB, et al., 2004 The novel marker, DOG1, is expressed ubiquitously in gastrointestinal stromal tumors irrespective of KIT or PDGFRA mutation status. Am. J. Pathol 165 (1), 107–113. [PubMed: 15215166]

Wondergem R, et al., 2001 Blocking swelling-activated chloride current inhibits mouse liver cell proliferation. J. Physiol 532 (3), 661–672. [PubMed: 11313437]

Wuytack F, Raeymaekers L, Missiaen L, 2002 Molecular physiology of the SERCA and SPCA pumps. Cell Calcium 32 (5), 279–305. [PubMed: 12543090]

Yang YD, et al., 2008 TMEM16A confers receptor-activated calcium-dependent chloride conductance. Nature 455 (7217), 1210–1215. [PubMed: 18724360]

Zayzafoon M, 2006 Calcium/calmodulin signaling controls osteoblast growth and differentiation. J. Cell. Biochem 97 (1), 56–70. [PubMed: 16229015]

Zhang W, Liu HT, 2002 MAPK signal pathways in the regulation of cell proliferation in mammalian cells. Cell Res. 12 (1), 9–18. [PubMed: 11942415]

Zheng JQ, Poo M. m., 2007 Calcium signaling in neuronal motility. Annu. Rev. Cell Dev. Biol 23 (1), 375–404. [PubMed: 17944572]

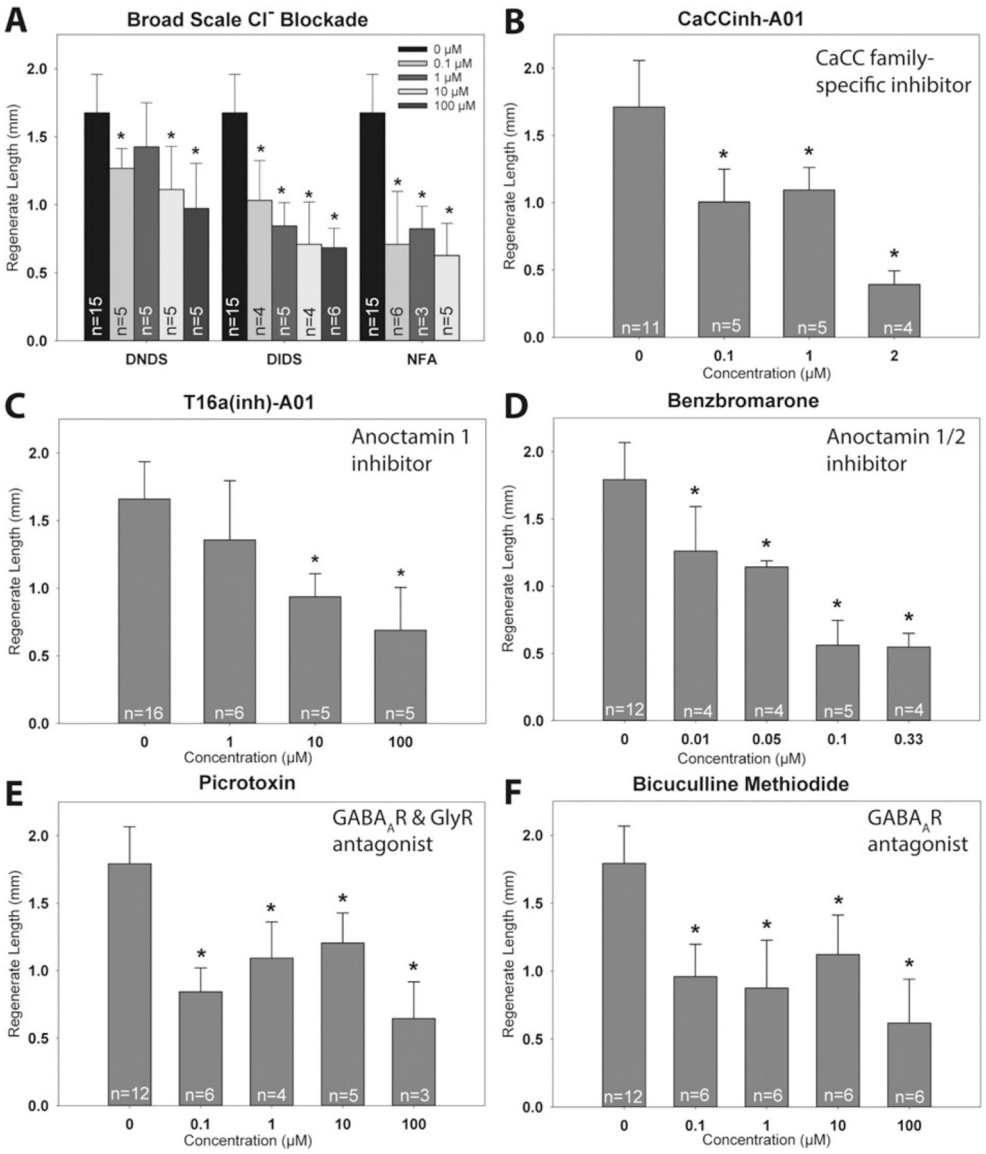

Fig. 1.

(A) All broad scale inhibitors of chloride channels (DNDS, DIDS and NFA) robustly reduced tail regeneration at concentrations of 100 nM and above. (B–D) Inhibitors of calcium activated chloride currents with CaCCinh-A01, T16a(inh)-A01 and Benzbromarone all reduced regenerative growth in a concentration dependent manner with maximal responses at 2, 100 and 0.33 µM respectively. (E & F) PTx and BCU were used to investigate the role of ligand-gated chloride channels and both exhibited robust inhibition of regeneration at all concentrations tested (* indicates $p < 0.05$ compare to control or concentration = 0; error bars are standard deviations, n values depicted on bar graphs represent biological replicates).

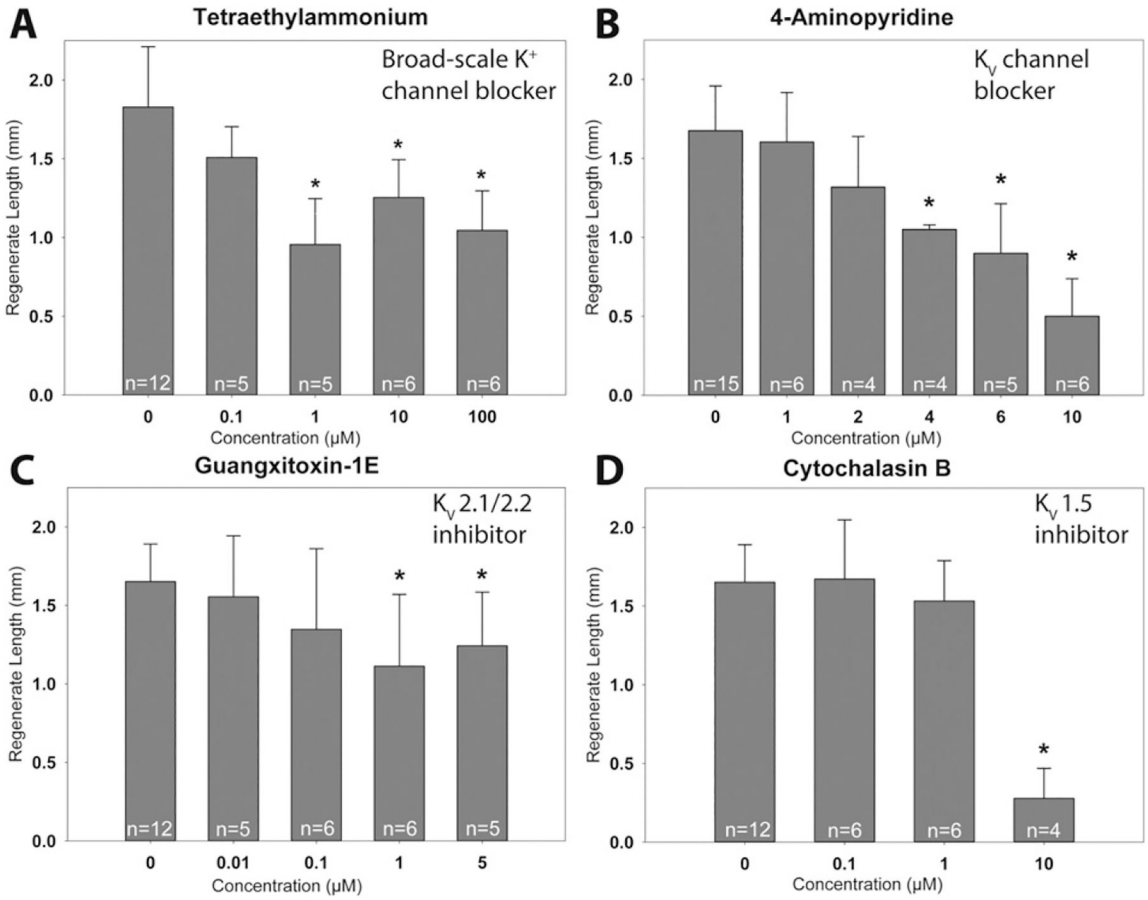

Fig. 2.

(A) While the broad scale potassium channel inhibitor TEA only reduced regenerative growth (B) the voltage-gated K^+ channel blocker 4-AP exhibited concentration dependent inhibition. (C) $K_V2.1/2.2$ channels that were inhibited with GTx-1E exhibited a slight reduction of regenerative growth at 1 and 5 μM but was lethal at all concentrations above 5 μM and (D) CB exhibited complete inhibition at 10 μM (* indicates $p < 0.05$ compare to control or concentration = 0; error bars are standard deviations, n values depicted on bar graphs represent biological replicates).

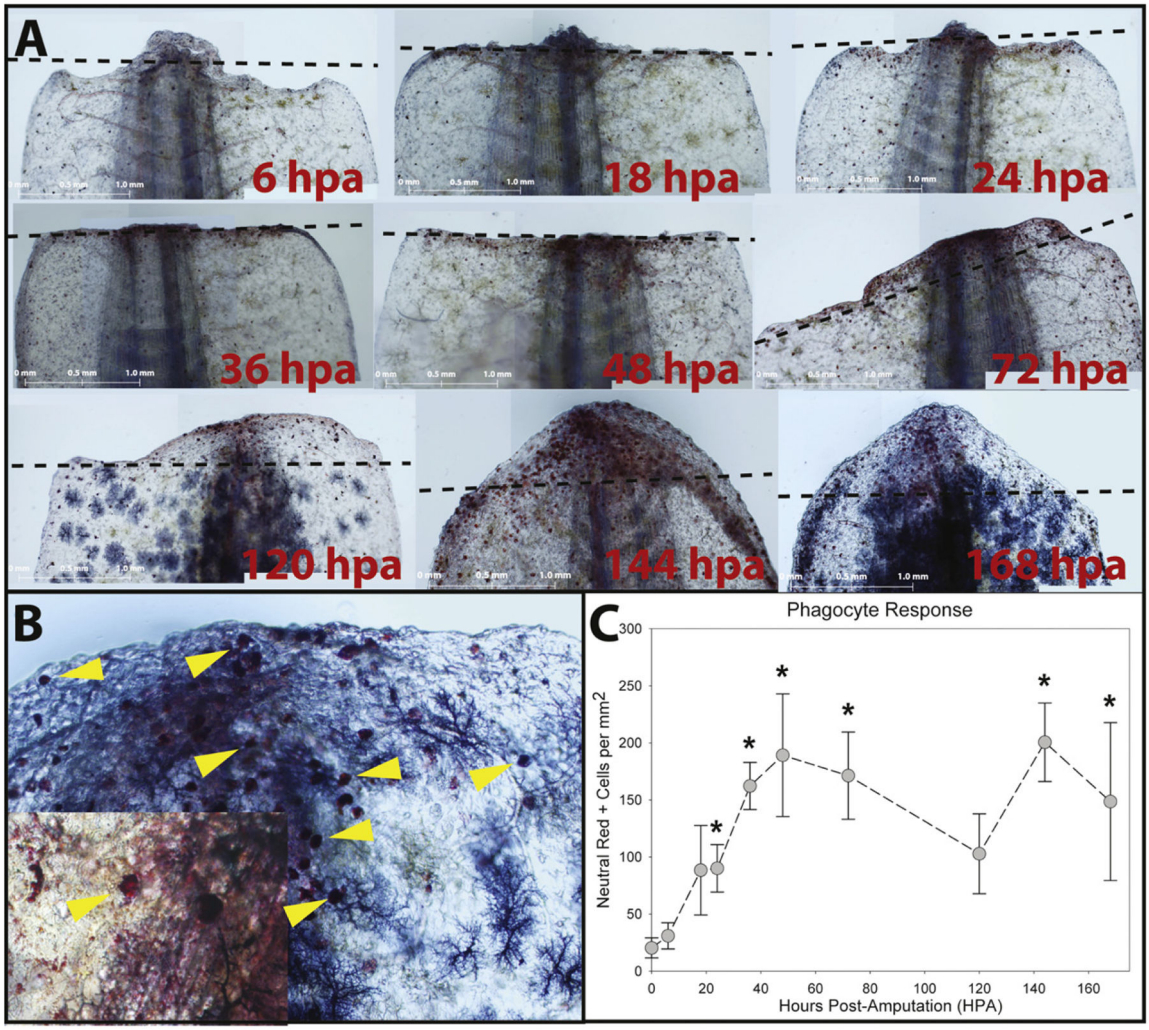

Fig. 3.

Phagocytes were stained in live regenerating axolotl embryos with neutral red at 6, 18, 24, 36, 48 (2 days), 72 (3 days), 120 (5 days), 144 (6 days) & 168 (7 days) hpa. Panel (A) depicts representative micrographs of each time point (amputation plane indicated by black dashed line) with enlarged photos in panels (B & B′) showing individual phagocytes. Representative (but not all) NR+ cells are indicated by yellow arrowheads. (C) Phagocytes were counted from 500 μM proximal of the amputation plane to the tip of the tail and normalized by tissue cross-sectional area. Phagocyte density steadily increased over the first few days following amputation peaking between days 2 and 3. This was followed by a trough in phagocyte density between days 3 and 5 that corresponded to increased tissue outgrowth, and then a second phagocyte density peak at day 6 (* indicates $p < 0.05$ compared to phagocyte density immediately following amputation; scale bars represent 1 mm; error bars are standard deviations). (For interpretation of the references to colour in this figure legend, the reader is referred to the web version of this article.)

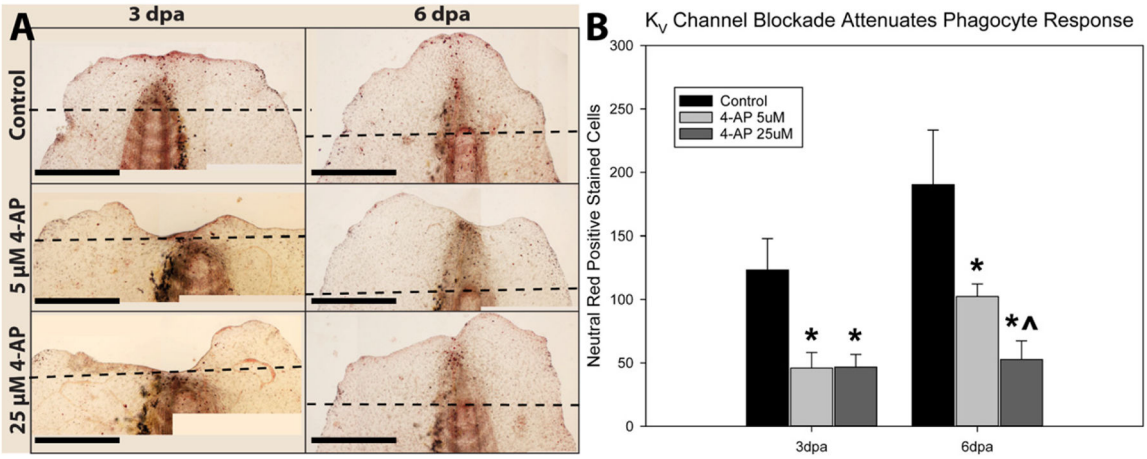

Fig. 4.

Phagocytes were stained in live animals with neutral red at 3 and 6 dpa. Panel (A) depicts representative micrographs of all time points and treatments (amputation plane indicated by black dashed line). (B) 4AP inhibits phagocyte activation and recruitment to the wound site at concentrations of either 5 or 25 µM. This response is concentration dependent at 6dpa but not 3dpa (* indicates $p < 0.05$ compared to control and ^ indicates $p < 0.05$ compared animals treated with 5 µM 4AP; scale bars represent 1 mm; error bars are standard deviations).

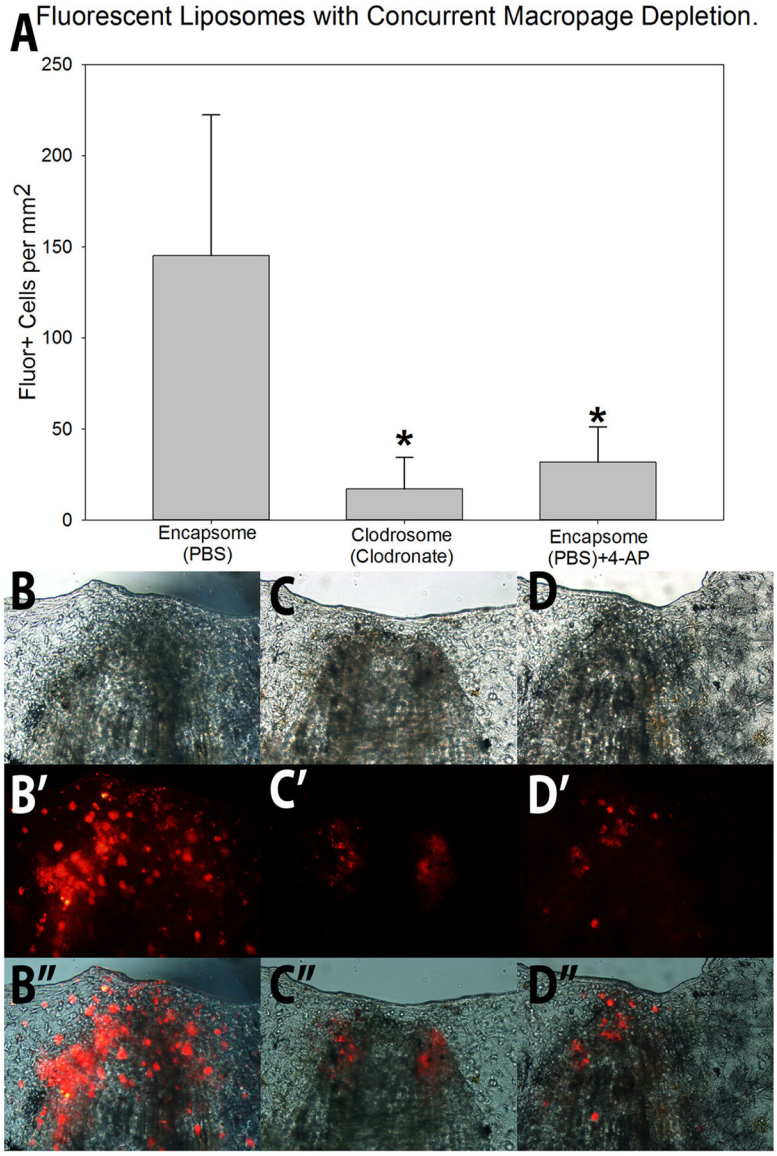

Fig. 5.

Phagocytes were labeled by IP injection of Fluorosome®-DiI 24 h prior to amputation and co-injected with either Encapsome® as a vehicle control (B-B″; $n = 10$), Clodrosome® for macrophage depletion (C-C″, $n = 15$) and a final group co-injected with Encapsome® and then incubated with 25 μM 4-AP following amputation for K_V channel blockade (D-D"; $n = 14$). (* indicates $p < 0.05$ compared to control; error bars are standard deviations) Both macrophage depletion prior to amputation (C-C″) and K_V channel blockade following amputation (D-D″) reduced the number of DiI+ cells at the wound site.

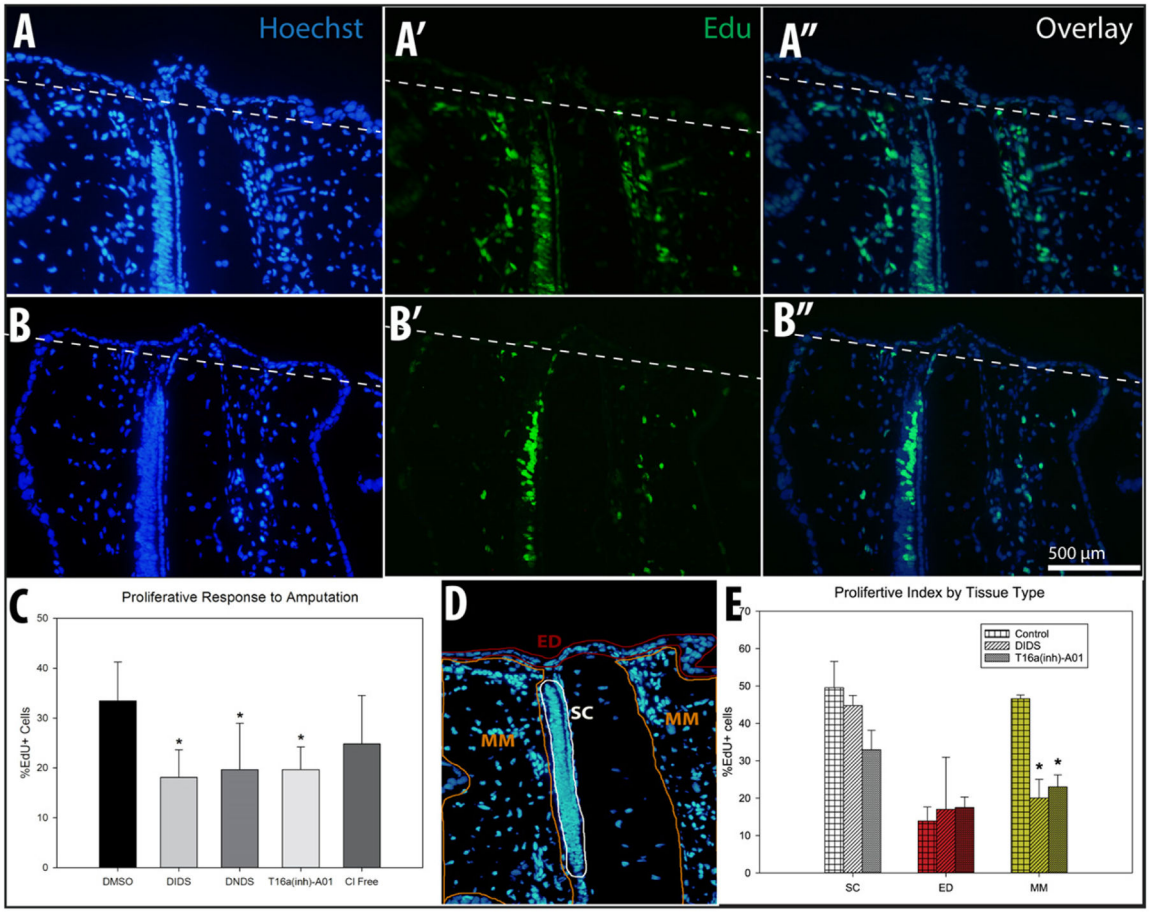

Fig. 6.

Compared to controls ($n = 4$) (A-A″), the proliferative response to amputation was reduced by broad scale chloride channel blockade with either DIDS ($n = 4$) or DNDS ($n = 5$) (C) as well as anoctamin-1 channel blockade with T16a(inh)-A01 ($n = 5$) (B-B″)) but not when animals were incubated in chloride free medium ($n = 5$) (C) (amputation plane indicated by white dashed line). Taken together these data suggest that chloride channel signaling is a critical step in the mechanism(s) driving proliferation in response to amputation. (* indicates $p < 0.05$ compared to control; error bars are standard deviations) (D&E) Neither DIDS nor T16a(inh)-A01 had an effect on proliferation in spinal cord (SC) or epidermal (ED) tissues. In mesenchymal tissues (MM) directly underlying the wound epidermis and within 500 µm of the amputation plane, proliferation was reduced from 46.6 ± 0.7% in control animals to either 20.0 ± 3.5% (DIDS) or 23.0 ± 2.9% (T16a(inh)-A01) in treated animals (* indicates $p < 0.05$ compared to control of same tissue type; error bars are standard deviations).

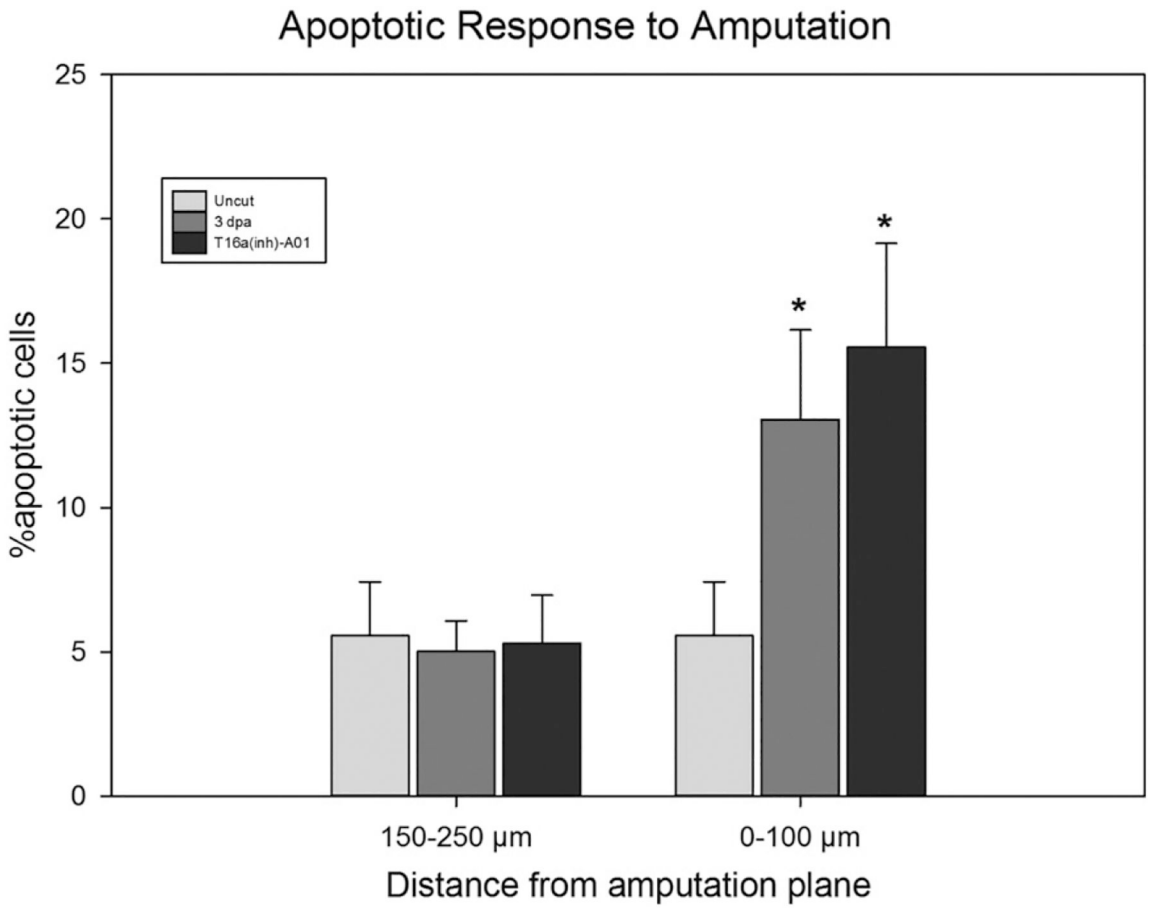

Fig. 7.

Apoptosis was assessed following amputation in 3 dpa animals and compared to apoptotic rates in tissue from un-amputated axolotl tails. Tissues were cut into transverse sections and then divided into groups consisting of sections of either from the tail tip to 100 µM distal of the amputation plane and a second group consisting of tissue from 150 to 250 µM distal of the amputation plane. No differenced were observed in the latter group but the former exhibited similar increases in apoptotic cells in both the control 3 dpa animals and 3 dpa animals treated with the Ano1 inhibitor (* indicates $p < 0.05$ compared to un-amputated tail tissue).

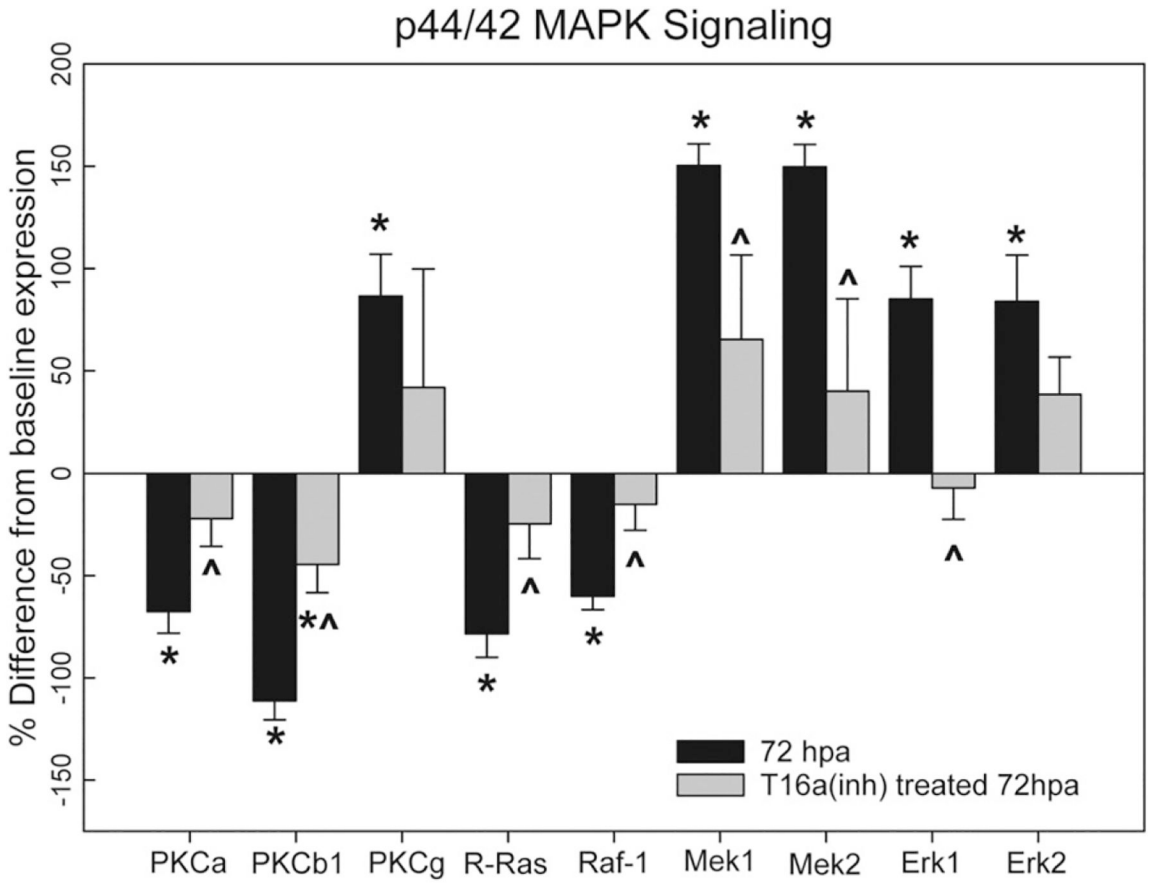

Fig. 8.

Quantitative Real-Time PCR was used to assess the mRNA expression of genes associated with the p44/42 MAPK (Erk 1/2) signaling pathway at 72 h post amputation (hpa) in regenerating axolotl tails and at the same time point in animals treated with 20 μM T16Ainh-A01. Expression in tail tissues from un-amputated animals was used as control/baseline. All genes other than PKCγ exhibit modulated expression at 3 dpa, which was attenuated by Ano1 blockade (* indicates $p < 0.05$ compared to control and ^ indicates $p < 0.05$ compared to normal 72 hpa animals; error bars are standard deviations).

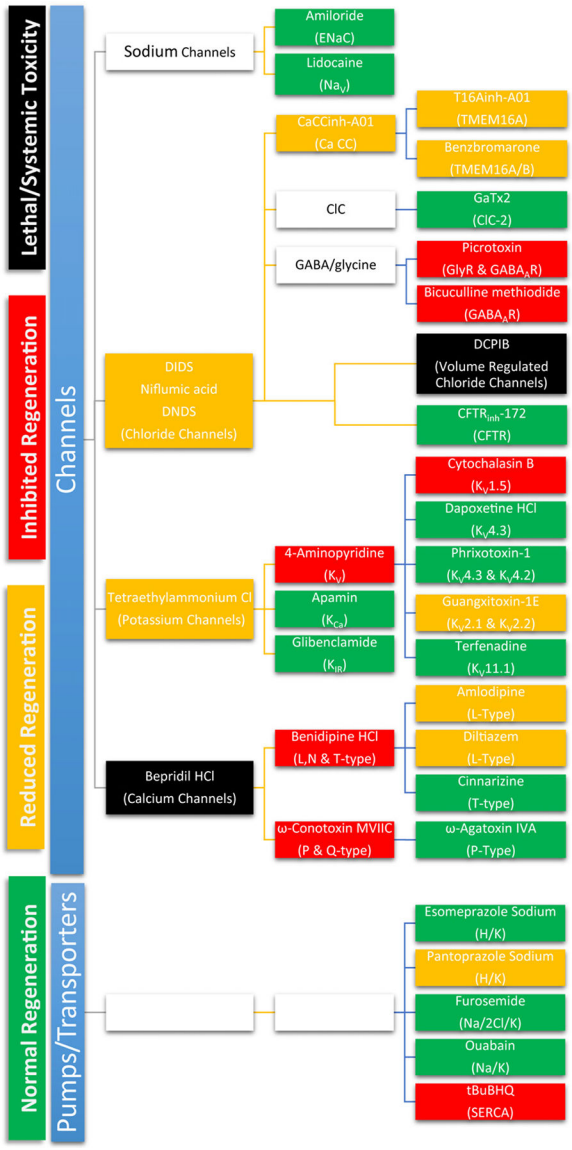

Fig. 9.

A comprehensive screen of ion channel blockers was used to identify specific channels involved in critical cellular processes of growth and regeneration such as proliferation, migration and differentiation. Drugs that did not affect regeneration are depicted in green, drugs that resulted in partial regeneration are depicted in yellow, drugs that completely inhibited regeneration (for any of the concentrations tested) are depicted in red and drugs that were lethal at all concentrations or caused systemic toxicity (identified by general atrophy, lethargy and/or tissue degeneration) are depicted in black. (For interpretation of the references to colour in this figure legend, the reader is referred to the web version of this article.)

Table 1

This table summarizes all compounds and the concentrations of each compound screened for an effect on regeneration. Every concentration of each compound was screened using 6 or more animals. Concentrations were deemed to be lethal and/or systemically toxic (**listed in bold**) if 60% or greater of the animals in the screen either died or exhibited characteristics of toxicity (anatomical abnormalities in the gills, reduced blood flow in gills, general atrophy and degeneration).

	Tier 1		**Tier 2**		**Tier 3**	
	Drug	**Concentrations (μM)**	**Drug**	**Concentrations (μM)**	**Drug**	**Concentrations (μM)**
Sodium			Amiloride	0.1, 1, 10 & 100		
			Lidocaine	0.1, 1, 10 & 100		
			Tetrodotoxin	0.01, 0.1, 1, 10 & **100**		
Chloride	DIDS	0.1, 1, 10 & 100	CaCCinh-A01	0.1, 1, 2, **4**, **6**, **8**, **10** & **100**	T16Ainh-A01	0.1, 1, 10 & 100
					Benzbromarone	0.01, 0.05, 0.1, 0.33, **0.66**, **1**, **10** & **100**
			ClC channels		GaTx2	0.001, 0.01, 0.1, 1 & **10**
	DNDS	0.1, 1, 10 & 100	Ligand gated Cl channels		Picrotoxin	0.1, 1, 10 & 100
					Bicuculine Methiodide	0.1, 1, 10 & 100
	Niflumic acid	0.1, 1, 10 & 100	Volume-sensitive anion channel		DCPIB	0.1, **1**, **10** & **100**
			Cystic fibrosis transmembrane receptor		$CFTR_{inh}$-172	0.1, 1, 10 & 100
Potassium	Tetraethylammonium	0.1, 1, 10 & 100	4-Aminopyridine	0.1, 1, 2, 4, 6, 8, 10 & 100	Cytochalasin B	0.001, 0.01, 0.1, **1** & **10**
					Dapoxetine	0.1, 1, 10 & **100**
					Phrixotoxin-1	0.0001, 0.001, 0.01, 0.1, **1** & **10**
					Guangxitoxin-1E	0.001, 0.01, 0.1, 1 & **10**
					Terfenadine	0.1, 1, 2, 4, 6, 8, **10** & **100**
			Apamin	0.01, 0.1, 1 & 10		
			Glibenclamide	0.1, 1, 10 & 100		
Calcium	Bepridil HCl	**0.1**, **1**, **10** & **100**	Benidipine HCl	0.1, **1**, **10** & **100**	Amlodipine	0.1, 1, 10 & **100**
					Diltiazem	0.1, 1, 10 & **100**
					Cinnarizine	0.1, 1, 10 & **100**
			ω-Conotoxin MVIIC	0.001, 0.01, 0.1, 1 & **10**	ω-Agatoxin	0.01, 0.05, **0.1**, **1** & **10**
Pumps/transporters					Esomeprazole	0.1, 1, 10 & 100
					Pantoprazole	0.1, 1, 10 & 100
					Furosemide	0.1, 1, 10 & 100

Tier 1		Tier 2		Tier 3	
Drug	**Concentrations (μM)**	**Drug**	**Concentrations (μM)**	**Drug**	**Concentrations (μM)**
				Ouabain	0.1, 1, 10, 50 & 100
				tBuBHQ	0.1, 0.5, 1, 2, **4**, **6**, **8**, **10** & **100**

Table 2

This table summarizes the primers used to measure gene transcription by quantitative real-time PCR.

Gene	Forward primer	Reverse primer
GAPDH	ACGTCTCTGTGGTTGACTTG	TTCCCTTCATTGGTCCATCAG
PKC-γ	GGCAGTCGTGAGATGAGTTT	ACCGATACAAGCTGAGTGAAG
PKC-α	CGTAGAATGCACGATGGTAGAA	TCCTCAGTTTGGAAGCAAGAA
PKC-β	CGCATGAAGCTATCCGACTT	CATAGAGCTCGTCAGTACCTTTC
RRAS	GTCCACATTAAGCCGGATCT	CCTACATAGACAGGTGCCAAA
RAF1	AGGAGACCAAGTTTCAGATGTT	GTCCCTGTGGATGATGTTCTT
MAPKK1	AGCTCCTGTGAAGCGTATTC	CCTAGATCTGCCCTGCATTT
MAPKK2	GAGGAAGGGAAACCGAACATAA	CTTAGCTCGTCTACAGCCAATC
MAPK1/ERK2	CGGGCACCAGAGATAATGTT	GGAAGATGGGTCTGTTAGATAGC
MAPK3/ERK1	CGCATTGGATCTGCTGGATAA	GGTCGTAGTACTGTTCCAGGTA